Streptomyces alleviate abiotic stress in plant by producing pteridic acids

Zhijie Yang,[a] Emil Strøbech,[a] Yijun Qiao,[a] Naga Charan Konakall,[b] Pernille Harris,[c] Gundela Peschel,[d] Miriam Agler-Rosenbaum,[d] Tilmann Weber,[e] Erik Andreasson,[b] Ling Ding[a,*]

[a] Department of Biotechnology and Biomedicine, Technical University of Denmark, Søltofts Plads bldg. 221, DK-2800 Kgs Lyngby, Denmark.
[b] Department of Plant Protection Biology, Swedish University of Agricultural Sciences, Sundsvägen 14, SE-230 53, Alnarp, Sweden.
[c] Department of Chemistry, Technical University of Denmark, Søltofts Plads bldg. 206, DK-2800 Kgs Lyngby, Denmark.
[d] Leibniz Institute for Natural Product Research and Infection Biology – Hans Knöll Institute (HKI), Beutenbergstr. 11a, 07745 Jena, Germany.
[e] Novo Nordisk Foundation Center for Biosustainability, Technical University of Denmark, Kemitorvet, Building 220, 2800 Kgs. Lyngby, Denmark.
*Corresponding author: Ling Ding lidi@dtu.dk

ABSTRACT

Soil microbiota confer fitness advantages to plants and increase crop resilience to drought and other abiotic stressors. However, there is little evidence on the mechanisms correlating a microbial trait with plant abiotic stress tolerance. Here, we report that a class of *Streptomyces* effectively alleviates the drought and salinity stress by producing new spiroketal polyketide pteridic acid H (**1**) and its isomer F (**2**). The bifunctional pteridic acid (*pta*) biosynthetic gene cluster (BGC), which is also responsible for the biosynthesis of the known antimicrobial elaiophylin, was confirmed by bioinformatic analysis and *in vivo* CRISPR base editing. Pteridic acids H and F exhibited profound effects in promoting root growth in Arabidopsis at a concentration of 0.5 ng mL^{-1} (1.3 nM) under abiotic stress, indicating they are a new class of plant stress regulators. Phylogenetic and geographical distribution analysis revealed that the *pta* BGC was mainly disseminated by vertical transmission and occasional horizontal gene transfer and is widely distributed in numerous *Streptomyces* in different environments. This discovery provides a new perspective for understanding plant-*Streptomyces* interactions and provides a novel, promising approach for utilising beneficial *Streptomyces* and their secondary metabolites in agriculture to mitigate the detrimental effects of climate change.

According to Food and Agriculture Organization (FAO), climate change generates considerable uncertainty about future water availability in many regions. Increased water scarcity under climate change will present a major challenge for climate adaptation, while sea-level rise will affect the salinity of surface and groundwater in coastal areas. Stress caused by climate change has led to increased agricultural losses and threatened global food security.[1,2] Drought is considered the most damaging environmental stress, which directly affects the entire growth period of plant seeds from germination to final fruiting.[3] Drought stress can lead to increased plant osmotic regulators, the inhibition of photosynthesis, and the change of plant endogenous hormone content.[4-6] Drought stress also induces reactive oxygen species (ROS), such as superoxide radicals, hydrogen peroxide, and hydroxyl radicals, leading to oxidative stress.[7] At high concentrations, ROS can cause damage at various tissue levels, for example, triggering lipid peroxidation and membrane degradation in plants.[8,9] Crop loss due to soil salinisation is another increasing threat to agriculture worldwide, which is more severe in agricultural land in coastal and arid regions.[10] Irrigation with saline water, low precipitation, and high evapotranspiration are key factors of the rapid salinisation of agricultural land.[11] These abiotic stresses of drought and salinity have brought unprecedented challenges to the development of crop farming. Compared to the heavy use of chemical fertilisers, the use of plant growth-promoting bacteria (PGPB) to improve plant growth under drought and salinity environments is more sustainable and gaining more attention.[12,13]

Soil microbial communities are critical to plant health and their resistance to both biotic and abiotic stressors, such as pathogens, drought, salinity, and heavy metal pollution.[14] A few studies have demonstrated that many beneficial soil bacteria harbour plant growth-promoting activities, *e.g.* by helping plants with disease suppression,[15] nutrient acquisition,[16] phosphorus uptake,[17] and nitrogen fixations.[18] Beneficial root microbiota also regulates biosynthetic pathways in the plant itself, leading to differential alterations in the plant metabolome in response to stresses.[19] *Streptomyces* are Gram-positive filamentous bacteria, widely distributed in soil and marine environments. While they have long been considered the richest source of bioactive secondary metabolites,[20] *Streptomyces* have recently drawn attention as a class of PGPB that help plants respond to adversity stress.[21] The growing evidence showed that *Streptomyces* can promote plant growth or tolerance to stressors in direct or indirect ways, by secreting plant growth regulator auxin (indole-3-acetic acid, IAA) and siderophores, inducing systemic resistance in plants, and regulating the rhizosphere microbiome via producing antibacterial compounds or signalling molecules.[22-24] Notably, the commercial product Actinovate® and Mycostop® are two *Streptomyces*-based formulations that have been widely used to suppress a wide range of diseases in a variety of crop groups as a biological fungicide/bactericide for the long term. Recently, the enrichment of *Streptomyces* has also been shown to play a subsequent role in the drought/salt tolerance of plants.[25] Despite the widespread claims of efficacy of inoculation of plant growth-promoting *Streptomyces*, the molecular basis of the growth-promoting effects and the key role of secondary/specialised metabolites in this process are largely unknown.

In our efforts searching for plant growth-beneficial *Streptomyces* strains, we found that *Streptomyces iranensis* HM 35 has profound beneficial effects on helping barley alleviate drought and salinity stress. The active components were identified as a new bioactive spiroketal polyketide pteridic acid H (**1**) and its isomer F (**2**) through large-scale fermentation and bioactivity-directed purification followed by NMR, MS, and X-ray crystallography. The abiotic stress mitigating effect of pteridic acids H and F have been confirmed on the model plant *Arabidopsis thaliana*, where it completely reversed both drought and salinity stress as phytohormone-like small biomolecules at concentrations as low as 0.5 ng mL^{-1} ($\approx$ 1.3 nM). Moreover, the biosynthetic gene cluster (BGC) of pteridic acids (*pta*) was identified and analysed *in silico* and functionally confirmed by in vivo CRISPR-based genome editing. We have furthermore surveyed the distribution of a total of 81 potential pteridic acid producers, which are widely distributed worldwide, especially in the coastal environment, suggesting their critical roles in ecology. In addition to *S. iranensis* HM 35, two other native pteridic acid producers, *Streptomyces violaceusniger* and *Streptomyces rapamycinicus* also showed impressive activity to stimulate barley seedlings' growth under drought and salinity conditions. Phylogenetic and comparative genomic analysis of *Streptomyces* harbouring the *pta* biosynthetic gene cluster suggested that these strains have evolutionary convergence in disseminating *pta* BGC through main vertical transmission and occasional horizontal gene transfer. In summary, we reveal a so far unknown strategy of *Streptomyces* to secret plant growth regulators that help plants cope with abiotic stress, which is a promising alternative solution for plant development and crop yields under the current climate change-induced environmental stresses.

Results and Discussion

Discovery of abiotic stress-mitigating *Streptomyces*. To model native *Streptomyces*-plant interactions under drought conditions, the pot experiments using soils supplemented with 20% (w/v) PEG-6000 were usually applied to simulate drought stress by reducing the water potential (Ψ_W) of the plant.[27] We found that the

rhizosphere-derived *S. iranensis* HM 35 exhibited significant activity in helping barley seedlings alleviate drought stress (Fig. 1a). Compared to the untreated control, the height of barley seedlings was significantly increased ($p < 0.0001$) and reached stress-free levels when culture broth of *S. iranensis* was added (Fig. 1b, Supplementary Fig. S1). The fresh and dry weight of barley seedlings was completely reversed when treated with *S.iranensis* under drought stress. In addition, *S. iranensis* also showed considerable activity in alleviating salinity stress mediated by 100 mM NaCl (Fig. 1a). The treatment of culture broth with *S. iranensis* significantly increased plant height, fresh weight, and dry weight of barley seedlings under salinity stress (Fig. 1c; Supplementary Fig. S1). Surprisingly, *S. iranensis* promoted the growth of barley seedlings even in non-stress condition, and the height, fresh weight, and dry weight were improved 9.2%, 35.1%, and 65.6%, respectively (Supplementary Fig. S1).

To reveal the potential bioactive components, we first characterised its genomic and metabolomic profiles through secondary metabolites BGCs annotation and liquid chromatography-tandem mass spectrometry (LC-MS/MS), respectively. Genome sequence analysis of *S. iranensis* revealed the presence of 50 putative secondary metabolites BGCs (Supplementary Tab. S1), and their corresponding products, hygrocin A, azalomycin F3a, rapamycin, elaiophylin, *etc.*, were detected by LC-MS/MS (Fig. 1d, Supplementary Fig. S2). However, a large number of metabolites of *S. iranensis* are still unknown. Since none of those known compounds or other *Streptomyces* natural products has been linked to plant abiotic stress-mitigating activities, this motivated us to scale up the fermentation and find the bioactive compounds.

Characterisation of the bioactive compound pteridic acid. To uncover the bioactive components, *S. iranensis* fermentation was scaled up to 175 litres and the culture broth was subjected to separation through open-column chromatography on Amberchrom CG161Me resin, silica gel, and Sephadex LH-20. Bioactivity-guided fractionation led to the isolation of bioactive compound **1** (15.0 mg) together with another structurally related compound **2** (4.0 mg) (Fig. 1e).

The bioactive component compound **1** was isolated as a white solid. Its formula of $C_{21}H_{34}O_6$ was deduced by *m/z* 383.2439 $[M+H]^+$ (calculated for 383.2428, Δ 2.84 ppm). The ^{1}H NMR spectrum exhibited signals for four olefinic protons (δ 7.33, 6.26, 6.13, 5.90) corresponding to two conjugated double bonds, four oxygen-bearing methines (δ 3.85, 3.69, 3.59, 3.43), five methyls, and other aliphatic protons. The ^{13}C NMR spectrum indicated the presence of one carbonyl group (δ 168.7) and one oxygen-bearing quaternary carbon (δ 103.2, C-11). The COSY spectrum established two partial substructures, which could be connected via a spiral function by analysing HSQC and HMBC correlations (Supplementary Fig. S3-S10). Compound **1** was crystallised in methanol solution, and the structure was determined via X-ray crystallography (Supplementary Fig. S11). Compound **1** was a new metabolite named pteridic acid H.

Compound **2**, a white solid, is an isomer of **1** since MS deduced the same molecular formula of $C_{21}H_{34}O_6$. The ^{1}H NMR spectrum exhibited signals for four olefinic protons (δ 7.16, 6.25, 6.07, 5.97) corresponding to two conjugated double bonds, four oxygen-bearing methines (δ 3.88, 3.66, 3.56, 3.32), five methyls, and other aliphatic protons. The ^{13}C NMR spectrum indicated the presence of one carbonyl group (δ 170.2) and one oxygen-bearing quaternary carbon (δ 103.2, C-11). HSQC and HMBC correlations confirmed a spiroketal skeleton. NOESY spectrum confirmed its relative configurations, where correlations between H-21 and H-13 and H-15, H-7 and H-12a, and H6, H-10, and Me-18 were observed. The key NOESY correlations between H-7 and H-12a revealed a different spiroketal structure than **1** (Supplementary Fig. S10, S12-S19). This can be reflected by the relative up-field NMR data for C-12 (δ 33.8 vs δ 37.4 in **1**). Compound **2** was identified as pteridic acid F, previously isolated from *Streptomyces pseudoverticillus* YN17707 and a marine-derived *Streptomyces* sp. SCSGAA 0027.[28,29]

Abiotic stress mitigation of pteridic acids *in planta*. Drought and salinity stress causes a series of characteristic responses in plants, of which the phytohormone abscisic acid (ABA) is involved in numerous developmental processes and adaptive stress responses.[30] Since pteridic acid H exhibited a comparable effect as ABA in preliminary barley growth experiments (Supplementary Fig. S20), we decided to conduct further experiments on the model plant *A. thaliana*. In the absence of abiotic stress, pteridic acid H, as well as ABA, significantly increased the root length and fresh weight of Arabidopsis seedlings, which was not observed in the group of pteridic acid F treatment (Fig. 2a, 2d). Under drought stress mediated by PEG-6000, pteridic acid H at a concentration of 0.5 ng mL^{-1} increased the root length and fresh weight of Arabidopsis seedlings by 54.5% and 89%, respectively, and its activity was significantly better than the ABA at the same molar concentration (Fig. 2b). The treatment of pteridic acid F also showed great activity in alleviating drought stress, and the root length and fresh weight were increased by 30.5% and 56.7%, respectively (Fig. 2e). Root architecture plays a vital role in plant adaptation to drought stress and deep roots enable plants to extract water from deep soil layers.[31] Intriguingly, unlike ABA, pteridic acid F could significantly enhance the lateral root growth of Arabidopsis seedlings, which was also observed in mung bean experiments (Fig. 2h, Supplementary Fig. S21).

In addition, pteridic acids H and F also showed significant activity in alleviating NaCl-mediated salinity stress (Fig. 2c). Compared to the non-treated Arabidopsis seedlings, the treatment of 0.5 ng mL^{-1} pteridic acids H and F increased root length by 74.0% and 61.8%, as well as fresh weight by 126.2% and 110.9%, respectively (Fig. 2f). Pteridic acid H also showed better alleviation activity for Arabidopsis seedlings than ABA under salinity stress. The previous study indicated that pteridic acids A and B might act as IAA-like plant growth promoters and induce the formation of adventitious roots in kidney beans.[28] Surprisingly, pteridic acids H and F exhibited completely different growth-promoting mechanisms with IAA through a distinct Arabidopsis phenotype, and they couldn't significantly promote the formation of adventitious roots in kidney beans in our studies (Supplementary Fig. S22). Except for drought and salinity stress, we also tested the $CuSO_4$-mediated heavy metal stress alleviation activity of pteridic acids in Mung beans. The results showed that the 1 ng mL^{-1} pteridic acid H was effective as ABA in helping Mung beans to relieve heavy metal stress (Supplementary Fig. S23). In conclusion, pteridic acids H and F are new, widely applicable potent plant growth regulators produced by *Streptomyces* to assist plants in coping with abiotic stress with an unusual mode of action and have great value for agriculture applications under climate change.

Biosynthesis of pteridic acids. The retro-biosynthesis analysis indicated that pteridic acids could derive from a modular type I polyketide synthase. A putative *pta* BGC was identified in the whole genome sequence of S. *iranensis* HM 35, which shows 87% antiSMASH similarity to the BGC of elaiophylin (BGC0000053 in MiBiG database).[32] The *pta* BGC spans approximately 56 kb and encodes 20 individual biosynthetic genes responsible for the biosynthesis of core polyketide backbones, precursor, glycosylated substituents, transporters, and regulators (Supplementary Tab. S2). The five consecutive type I polyketides genes within the *pta* BGC consist of one loading module and seven extender modules, which are sequentially extended to form a linear polyketide chain by ketosynthase (KS) domain, acyltransferase (AT) domain, acyl carrier protein (ACP), with additional ketoreductase (KR), dehydratase (DH), and enoyl reductase (ER) domains. The substrate specificity predictions for individual AT domains (Supplementary Tab. S3) fit well with pteridic acids structure. KR domains are present in all extension modules. The last "Asn" residue is absent in the conserved Lys-Ser-Tyr-Asn tetrad of the KR domain in module 3 (PtaB) (Supplementary Fig. S24), which is predicted to be inactive. This is consistent with the nonreduced carbonyl group on the α-carbon in module 3. The first DH domain in module 1 is inactive since it does not have a conserved active motif LxxHxxGxxxxP (Supplementary Fig. S25). Following the thioesterase-mediated release of the polyketide chain, the 6,6-spiroketal core structure is likely formed by spontaneous spiroketalisation of the carbonyl group on C11 and the two hydroxyl groups on C17 and C25. Following a loss of H_2O, two differentially oriented spirocyclic rings were formed to yield pteridic acids F and H (Fig. 3a). Remarkably, pteridic acid H showed molecular instability under extreme conditions. In the water solution with high temperature (65℃) or acidity (pH = 3), pteridic acid H is transformed into pteridic acid F (Supplementary Fig. S26). A similar spontaneous transformation from (*S*) to (*R*) chirality at the centre of the spiroketal ring was also observed in 6,6-spiroketal avermectin.[33]

DSB-free CRISPR base editing in *S. iranensis* HM 35. To experimentally confirm the *in silico* BGC prediction, we applied the highly efficient double-strand break (DSB)-free CRISPR base editing tool CRISPR-cBEST.[34] Previous studies have shown that *S. iranensis* HM 35, as a non-model strain, is hard to genetically manipulate through intergeneric conjugation.[35] Therefore, the conjugation process was systematically optimised in this study (Supplementary Fig. S27). The core polyketide synthase *ptaA* was targeted and inactivated by converting a TGG (Trp) codon at position 916 into the stop codon TAA using CRISPR base editing. The editing event was confirmed by PCR amplification and Sanger sequencing of the editing site (Fig. 3c). As expected, the production of both pteridic acids and elaiophylin was abolished in *S. iranensis* HM 35/Δ*ptaA* (Fig. 3c). Plant experiments showed that the treatment of *S. iranensis* HM 35/Δ*ptaA* fermentation suspension led to the abolishment of the abiotic stress mitigating effects under 20% (w/v) PEG-6000-mediated drought stress and 100 mM NaCl-mediated salinity stress, compared with the native strain (Fig. 1b and 1c).

Interestingly, based on isotope-labelled precursor feeding and partial cosmid sequencing-based bioinformatics prediction, this BGC has long been inferred to be responsible for the biosynthesis of the antibacterial elaiophylin.[36,37] In 2015, Zhou et al. reported that the thioesterase (TE) domain in module 7 (PtaE) catalyse the formation of symmetrical diolide using two units of linear elaiophylin monomeric seco acid (Fig. 3b).[38] To confirm whether the biosynthesis of pteridic acids is also thioesterase-dependent, site-specific mutations of residues Met-Glu-Asp to Ile-Lys-Met were introduced into the active sites of the TE domain *in vivo* (Supplementary Fig. S28).[39] The LC-MS/MS analysis showed that the mutant strain (M2089I+E2090K+D2091M) no longer produced pteridic acids and elaiophylin. Hence, we provide additional evidence via *in vivo* inactivation and site-directed mutagenesis. Co-production of the plant growth-regulating pteridic acids and the antimicrobial

elaiophylin through a shared BGC is intriguing and points to joint efforts in helping plants cope with biotic and abiotic stress.

Geographical distribution of pteridic acid producers. To reveal whether it is a universal phenomenon for pteridic acid producers to help plants cope with abiotic stress, we investigated the natural distribution of *Streptomyces* possessing the *pta* BGC. We surveyed available gene cluster family (GCF) data for all bacteria in the BiG-FAM database.[40] We found that *pta* BGC (GCF_02696) is strictly restricted to the *Streptomyces* genus. In addition, a total of 55 BGCs with high similarity to the *pta* BGC were detected by BiG-SCAPE,[41] among a total of 9,386 type I polyketides BGCs in 1,965 *Streptomyces* from the NCBI assembly database. Through literature supplementation and data dereplication of other reported producers without sequence information, at least 81 *Streptomyces* are known to produce pteridic acids/elaiophylin or have specific *pta* BGC so far (Supplementary Tab. S4). Based on the known sampling geographic information, the geographic distribution of *pta*-containing *Streptomyces* was determined (Fig. 4a). Many of these strains have been isolated in the coastal high salinity area, and some of these have been described to have remarkable biocontrol capabilities. For example, *Streptomyces* sp. AgN23 activates Arabidopsis defence responses to fungal pathogen infection by secreting plant elicitors,[42] *Streptomyces rhizosphaericus* 0250 and *Streptomyces* sp. 5-10 displayed significant biocontrol potential to fusarium wilt of bitter gourd.[43,44]

To further confirm the potential plant growth-promoting activity of pteridic acid producers, two other rhizosphere-derived *Streptomycetes*, *S. violaceusniger* Tu 4113 and *S. rapamycinicus* NRRL 5491, were cultivated and fermented with ISP2 liquid medium. The GNPS molecular networking analysis of both culture broths revealed that they shared similar metabolite profiles, and the LC-MS/MS showed that they produced **1** and **2** (Supplementary Fig. S29).[45] Treatment with both culture broths on barley also exhibited significant plant growth-promoting activities under both drought and salinity stress conditions (Fig. 4b and 4c).

Phylogenetic and evolutionary analysis of *pta* BGC. Previous studies have shown that horizontal gene transfer is an integral driver of BGC evolution, revealing the independent processes of species phylogeny and BGCs distribution.[46] However, vertical inheritance also influences BGCs evolutionary dynamics, evident from BGCs conservation among closely related strains.[47] Understanding the evolutionary relationship among strains and their specialised metabolites also helps us realise the ecological roles of small molecules in constructing microbe-plant systems. To explore the evolutionary clues and potential ecological niche of pteridic acid producers, we investigated these producers with other *Streptomyces* through phylogenetic analysis. 16S rRNA genes and three high-resolution *Streptomyces* housekeeping genes, *trpB* (tryptophan synthase subunit beta) and *rpoB* (RNA polymerase subunit beta), were used to assess the relatedness of the potential producers of pteridic acids (Fig. 5a; Supplementary Fig. S30). The results revealed that, except for *S. albus* DSM 41398, other *pta*-containing *Streptomyces* cluster together and are distinct with divergent lineages. The strict congruence among the trees of the housekeeping genes indicated dominant vertical transmission and potential horizontal gene transfer of the *pta* BGC in *Streptomyces*. To further confirm this hypothesis, 15 *pta*-containing *Streptomyces* with complete genome sequences, including distinct strain *S. albus* DSM 41398, were selected to conduct the comparative genomics investigation.

The genetic diversity in these *Streptomyces* strains was initially revealed using genome sequence similarity analysis. Except for *S. albus* DSM 41398 and *Streptomyces* sp. NA02950, we found a high average nucleotide identity of the aligned region (ANI) and alignment percentage (AP) among these strains (Supplementary Fig. S31), indicating that they are closely related. Genome synteny analysis revealed that partial genome rearrangements happened among strains even with high sequence similarities (Supplementary Fig. S32). Notably, the *pta* BGC in *S. albus* DSM 41398 (*pta-alb*) is located at the end of the chromosome, the highly variable region in *Streptomyces*, suggesting its existence by accepting heterologous biosynthetic gene fragments. The nucleotide sequence alignment of *pta* BGC results showed that even though *pta-alb* is at the end of the chromosome, it's still relatively complete, and the similarity of core genes is proportional to evolutionary relatedness (Fig. 5b). The metabolite profile of *S. albus* DSM 41398 also confirmed the integrity of the *pta-alb* biosynthetic gene cluster by detecting the production of elaiophylin and pteridic acid H (Supplementary Fig. S33).

To further assess the biosynthesis diversity in remaining genetically related strains, we performed a BGCs similarity analysis. Characterising the relationship between their secondary metabolites, BGCs, revealed that these vertically inherited *Streptomyces* also harbour striking similarities (Fig. 5c, Supplementary Fig. S34). These *Streptomyces* strains were also described as a specific phylogenetic lineage with the highest BGC abundance and largest genome size across diverse *Streptomyces-type* strains.[48] There is currently some evidence suggests potential complex cross-BGC regulation in this class of *Streptomyces* strains: Jiang et al. demonstrated that a TetR family transcriptional regulator, GdmRIII, controls the biosynthesis of geldanamycin and elaiophylin meanwhile, in *Streptomyces autolyticus* CGMCC 0516.[49] Recently, He

et al. found that the rapamycin BGC-situated LAL family regulator RapH co-ordinately regulated the biosynthesis of both rapamycin and elaiophylin in *S. rapamycinicus* NRRL 5491.[50] Although these reports correspond to cross-regulation between evolutionarily conserved BGCs, more detailed mechanisms need to be studied. Combining phylogenetic and comparative genomics analysis, we can expect that the strain *S. albus* DSM 41398 is evolutionarily the most distinct member from other *pta*-containing *Streptomyces* and obtained the *pta* BGC via horizontal gene transfer. However, most *pta*-containing *Streptomyces* have vertically inherited *pta* and some other gene clusters from their ancient ancestors that may be ecologically important and rarely studied.

Conclusion

Given climate change and soil degradation, plant growth-promoting bacteria are receiving significant attention. Deciphering the molecular mechanism is key to understanding the complex plant microbiota interaction. Here, we present a novel example that *Streptomyces* can secrete a family of secondary metabolites, pteridic acids, to help various plants cope with abiotic stress. The unique evolutionary pattern indicated a vertical gene transmission, while the wide geographic distribution of *pta*-containing *Streptomyces*, especially in harsh environments, revealed their potential ecological role in helping plants with abiotic stress mitigation. Knowledge of the bacterial metabolite-mediated alteration of plants in response to environmental stress will open new avenues for utilising *Streptomyces* to rewild plant microbiomes and improve plant abiotic stress resistance and health.[51]

Methods

Strains, plasmids, and cultivation. *S. iranensis* HM 35 was initially isolated from a rhizosphere soil sample at a depth of 10 cm in Isfahan city, Iran. All strains and plasmids used in this study were listed in Supplementary Tab. S5. All *Escherichia coli* strains were grown in liquid/solid LB medium (5.0 g/L yeast extract, 10.0 g/L peptone, 10.0 g/L NaCl) at 37°C. All *Streptomyces* strains were grown on SFM medium (20.0 g/L, mannitol, 20.0 g/L soya flour, 20.0 g/L agar), and the SFM medium with the addition of 120 mM calcium chloride solution was used for the step of conjugation at 28°C. The ISP2 medium (4.0 g/L yeast extract, 10.0 g/L malt extract, 4.0 g/L dextrose, and 1.0 L distilled water) was used for liquid fermentation of all *Streptomyces* strains used in plant assay and metabolomics analysis. Appropriate antibiotics were supplemented with the following working concentrations: apramycin (50 µg/mL), chloramphenicol (25 µg/mL), and kanamycin (50 µg/mL). All *Streptomyces* strains were obtained from the German Collection of Microorganisms and Cell Cultures GmbH (DSMZ). All chemicals utilized in this study were from Sigma, USA.

Metabolomics analysis. Ultra-high-performance liquid chromatography–diode array detection–quadrupole time-of-flight mass spectrometry (UHPLC–DAD–QTOFMS) was carried out on the Agilent Infinity 1290 UHPLC system (Agilent Technologies, Santa Clara, CA, USA). The 250 × 2.1 mm i.d., 2.7 µm, Poroshell 120 Phenyl Hexyl column (Agilent Technologies, Santa Clara, CA) was used for separation. The 2-µL samples were eluted at a flow rate of 0.35 mL min^{-1} using a linear gradient from 10% acetonitrile in Milli-Q water buffered with 20 mM formic acid increasing to 100% in 15 min. Each starting condition was held for 3 min before the next run. Mass spectrometry detection was performed on an Agilent 6545 QTOF MS equipped with Agilent Dual Jet Stream electrospray ion source (ESI) with a drying gas temperature of 160°C, a gas flow of 13 L min^{-1}, sheath gas temperature of 300°C, and flow of 16 L min^{-1}. The capillary voltage was set to 4000 V and the nozzle voltage to 500 V in positive mode. MS spectra were recorded as centroid data at an m/z of 100-1700, and auto MS/HRMS fragmentation was performed at three collision energies (10, 20, and 40 eV) on the three most intense precursor peaks per program. LC-MS/MS data were analysed with MassHunter software (Agilent) and compared with known compounds and crude extract spectral libraries stored in the GNPS platform.[45] The precursor and fragment ion mass tolerance were set as 0.1 Da and 0.02 Da, respectively. In addition, the minpairs cos was set as 0.65, and the minimum matched fragment ions were set as 6.0. The metabolites profile of wild-type *S. iranensis* HM 35 was visualised by MS-Dial 4.9.2.[52]

Large-scale fermentation and isolation. *S. iranensis* HM 35 was cultivated in medium 2 (3.0 g/L $CaCl_2 \cdot 2H_2O$, 1.0 g/L citric acid/Fe III, 0.2 g/L $MnSO_4 \cdot H_2O$, 0.1 g/L $ZnCl_2$, 0.025 g/L $CuSO_4 \cdot 5H_2O$, 0.02 g/L $Na_2B_4O_2 \cdot 10H_2O$, 0.01 g/L $NaMoO_4 \cdot 2H_2O$, and 20.0 g/L oatmeal in 1.0 L distilled water), at 175 L filling volume in a 300 L fermentation vessel (Sartorius). The fermentation was carried out for 6 days with aeration of 25-50 L min^{-1}, stirring at 200 rpm with a temperature of 28°C and at a pH range of 5.4-6.4. The fermentation broth was separated, filtered, and loaded onto an Amberchrom CG161Me resin LC column (200 × 20 cm, 6 L). Elution with a linear gradient of H_2O-MeOH (from 30% to 100% v/v, flow rate 0.5 L min^{-1}, in 58 min) afforded seven fractions (A-G). Fraction G was firstly fractionated by silica gel chromatography with a CH_2Cl_2/CH_3OH gradient to yield 16 fractions, F01-F16. F07 was separated by a Sephadex LH-20 (MeOH) column, and twelve sub-fractions F07a-l were obtained. From F07e, **1** (15.0 mg) and **2** (4.0 mg) were obtained by repeated HPLC RP-C_{18} (CH_3CN/H_2O as gradient).

Petridic acid H (**1**): white solid; $[\alpha]_D^{20}$ 81 (0.32 mg/mL, CH_3OH), UV/vis (CH_3CN/H_2O) λ_{max} (%) 262 nm; IR (ATR) ν_{max} 2967, 2934, 2879, 1712, 1642, 1600, 1458,

1410, 1383, 1300, 1266, 1223, 1187, 1142, 1109, 1058, 1002, 973 cm^{-1}; (+)-HR-ESI-MS *m/z* 383.2439 $[M+H]^+$ (calcd for $C_{21}H_{35}O_6$, 383.2428). ^1H NMR and ^{13}C NMR see Supplementary Tab. S6.

Petridic acid F (**2**): white solid; $[\alpha]_D^{20}$ -18 (10 mg/mL, CH_3OH), UV/vis (CH_3CN/H_2O) λ_{max} (%) 264 nm; IR (ATR) ν_{max} 2968, 2931, 2877, 1692, 1643, 1618, 1458, 1410, 1380, 1299, 1270, 1188, 1138, 1106, 1059, 1002, 973, 850 cm^{-1}; (+)-HR-ESI-MS *m/z* 383.2433 $[M+H]^+$ (calcd for $C_{21}H_{35}O_6$, 383.2428). ^1H NMR and ^{13}C NMR see Supplementary Tab. S7.

Structure identification. NMR spectra were recorded on an 800 MHz Bruker Avance III spectrometer equipped with a TCI CryoProbe using standard pulse sequences. NMR data were processed using MestReNova 11.0. UHPLC-HRMS was performed on an Agilent Infinity 1290 UHPLC system equipped with a diode array detector. UV-Vis spectra were recorded from 190 to 640 nm. Specific rotations were acquired using Perkin-Elmer 241 polarimeter. IR data were acquired on Bruker Alpha FTIR spectrometer using OPUS version 7.2. TLC analysis was performed on silica gel plates (Sil G/UV_{254}, 0.20 mm, Macherey-Nagel). The Biotage Isolera One Flash Chromatography system was used for flash chromatography and performed on silica gel 60 (Merck, 0.04–0.063 mm, 230–400 mesh ASTM). Sephadex LH-20 was from Pharmacia. All solvents and chemicals used for HRMS and chromatography were VWR Chemicals LC-MS grade.

Crystal Structure Determination. X-ray data collection of **1** was performed on an Agilent Supernova Diffractometer using CuKα radiation. Data were processed and scaled using the CrysAlisPro software (Agilent Technologies). The structure was solved using SHELXS and refined using SHELXL. Hydrogen atoms were included in ideal positions using riding coordinates. The absolute configuration was determined based on the Flack parameter. Crystal Data for **1**: $C_{21}H_{34}O_6$, Mr = 382.50, monoclinic, a = 8.4619(1) Å, b = 15.6161(2) Å, c = 8.4994(1) Å, α = 90.00°, β = 107.768(1)°, γ = 90.00°, V = 1069.55(2) Å3, T = 120(2) K, space group P21, Z = 2, μ(Cu Kα) = 0.698 mm–1, 17514 reflections collected, 4275 independent reflections (Rint = 0.0226, Rsigma = 0.0155). The final R1 values were 0.0249 (I > 2σ(I)). The final wR2 values were 0.0648 (I > 2σ(I)). The final R1 values were 0.0252 (all data). The final wR2 values were 0.0651 (all data). The goodness of fit on F2 was 1.057. The Flack parameter is 0.13(10) (CCDC Deposition Number: 1984025).

Genetic manipulation. All primers used were synthesised by IDT (Integrated DNA Technologies, USA) and listed in Supplementary Tab. S8. Plasmids and genomic DNA purification, polymerase chain reaction (PCR), and cloning were conducted according to standard procedures using manufacturer protocols. PCR was performed using OneTaq Quick-Load 2X Master Mix with Standard Buffer (New England Biolabs, USA). DNA assembly was done by using NEBuilder HiFi DNA Assembly Master Mix (New England Biolabs, USA). DNA digestion was performed with FastDigest restriction enzymes (Thermo Fisher Scientific, USA). NucleoSpin Gel and PCR Clean-up Kits (Macherey-Nagel, Germany) were used for DNA clean-up from PCR products and agarose gel extracts. One Shot Mach1 T1 Phage-Resistant Chemically Competent *E. coli* (Thermo Fisher Scientific, USA) was used for cloning. NucleoSpin Plasmid EasyPure Kit (Macherey-Nagel, Germany) was used for plasmid preparation. Sanger sequencing was carried out using a Mix2Seq Kit (Eurofins Scientific, Luxembourg). All DNA manipulation experiments were conducted according to standard procedures using manufacturer protocols.

Gene inactivation and site-directed mutagenesis. To use the pCRISPR-cBEST for base editing applications, an oligo was designed as Del-ptaA by the online tool CRISPy-web, and the pCRISPR-cBEST plasmid was linearised by *Nco*I. Mixing the linearised pCRISPR-cBEST plasmid and Del-ptaA with the NEBuilder HiFi DNA Assembly Master Mix (New England Biolabs, USA). The linearised pCRISPR-cBEST plasmid was then bridged by Del-ptaA, ending with the desired pCRISPR-cBEST/Δ*ptaA*. Chemically-competent *E. coli* were transformed with the recombinant plasmid and confirmed via PCR amplification (program: 94°C for 30 s, followed by 30 cycles consisting of 94°C for 15 s; 54°C for 15 s; 68°C for 40 s, and 68°C for 2 min) and Sanger sequencing. The experimental procedure for site-directed mutagenesis for the TE domain is the same as described above. The *E. coli-Streptomyces* conjugation experiment was conducted according to the modified protocol in this study, and the mutant *Streptomyces* strains were also confirmed by PCR and Sanger sequencing.

Arabidopsis assay. *A. thaliana* ecotype Columbia (Col-0) was used to test the effects of pteridic acid treatment under drought stress mediated by PEG-6000 (Duchefa Biochemie BV) and salinity stress mediated by NaCl (Duchefa Biochemie BV). The modified Murashige & Skoog medium (2.2 g/L Murashige & Skoog medium including B5 vitamins, 5.0 g/L of sucrose, 250 mg/L MES monohydrate, 7.0 g/L agar, and adjusted pH to 5.7 with KOH) was used in this study. PEG-6000 (15% w/v) was dissolved in water and filtered through 0.2-micron Sartorius Minisart™ Plus Syringe Filters (Fisher Scientific). 50 mL of the filtered solution was overlaid onto the surface of solidified Murashige & Skoog medium. The plates were left for 24 h to diffuse the PEG into the Murashige & Skoog medium. NaCl was added

to the medium to a final concentration of 80 mM for the salinity stress alleviation test. The pure compound pteridic acids H and F (0.50 ng/mL), IAA (0.23 ng/mL), and ABA (0.34 ng/mL) were mixed with different media to a final concentration of approximately 1.3 nM and poured into the plates. Seeds were surface sterilised by washing with 70% ethanol for 2 min, then in sterilisation solution (10% bleach) for 1 min by inverting the tubes, and finally washed five times with sterilised water. The seeds were stratified for 2 days at 4°C in the dark. Sterilised seeds were placed in Petri dishes (approx. 100 seeds per Petri dish) on Murashige & Skoog medium and grown for 3-4 days in the vertical position in a culture chamber at 22°C under standard long-day conditions (16/8 h light/dark photoperiod). After three days of growth, seedlings with similar root lengths (7-10 mm) were transferred to square plates containing Murashige & Skoog medium (control) or Murashige & Skoog medium supplemented with 15% (w/v) PEG-6000 or 80 mM NaCl. 16 seedlings were used per replicate for each treatment. The initial position of the plant root tip was marked with a marker. The plants were grown in the vertical position under standard long day conditions (22°C, 16/8h light/dark) for 8 days, and then each plate was scanned using Image Scanner. Primary and lateral root lengths and the total plant weight were then scored. The primary and lateral root length measurements were performed by analysing pictures with the Image J software. Fresh weight measurements were estimated using a precision balance. Whole 8-day-old plants grown in the medium were removed using forceps, dried in tissue paper, and then weighed using a precision balance.

Barley and mung beans assay. The pteridic acid *Streptomyces* producers were tested for their effects on barley cultivars Guld grown in soil. *S. iranensis* HM 35, *S. rapamycinicus* NRRL 5491, and *S. violaceusniger* Tu 4113 were cultivated in ISP2 medium for 7 days at 28˚C. 500 µL culture broth (ca. 3 x 10^9 CFU/mL) was added to 100 g sand soil and well mixed. For pure substances, 10 nM pteridic acid H and ABA were added into a 50 mL Falcon tube containing 40 mL garden soil. Treated soils were infiltrated with water, 20% PEG-6000 solutions to simulate drought soil environments, and 100 mM NaCl solutions to simulate salinity soil environments. Barley seeds were rinsed in distilled water and sterilised with 1% sodium hypochlorite for 15 min. They were then washed with distilled water and germinated in distilled water at 24°C for 2 days. Barley seeds were planted in each plastic pot (5cm x 5cm x 6cm, six seedlings per pot) or 50 mL tube supplemented with different treated soil and grown at 24 ± 2°C, 8h dark/16h light in the growth chamber for 7 days. Plant height (cm) was measured as the aerial part of the plant, and the fresh shoot weight (g) and fresh root weight (g) of each seedling were measured separately. Then, the seedlings were dried in the hot-air oven at 70°C for 6 h to obtain the dry shoot and dry root weights (g). Mung beans were pre-germinated and placed on top of the modified Murashige & Skoog medium agar, supplemented with 10 mM CuSO4, with 1.0 ng/mL pure substances. For the drought assay, a solution of 20% (w/v) PEG-6000 was absorbed into a cotton cloth. Mung beans were placed on top of the cloth. All Mung beans were grown in the dark at 24 ± 2°C for 4 days.

Kidney beans assay. The seeds of kidney beans (appr. 2 cm in length, from organic farming) were firstly sterilised successively with ethanol (70% v/v) and sodium hypochlorite (5% v/v), each for 2 min and then rinsed with sterile Milli-Q water (three times). The sterilised seeds were cultivated on modified Murashige & Skoog agar plates for 3-4 days. After germination, the seedlings (with 1.5-2 cm-long roots) were soaked in 10 mL aliquots of testing compounds (pteridic acids H and F, 1.0 ng/mL, dissolved in sterile Milli-Q water) in ultra-clear polypropylene containers (ø 34 mm, vol. 20 mL) with polyethylene caps. The control group was treated with 10 mL sterile Milli-Q water. For each treatment, three repetitions (containers) were used, and each repetition included four seedlings. After 24 h, the seeds were transferred into a cut square petri dish, put on the top layer of sandy soil, and then incubated vertically in a growth chamber (24/22°C, day/night cycle of 16/8 h, 50%, 60%, 70%, 100% of circulated wind velocity for 12 h, 2 h, 2h, 8h) for 7 days. Solutions of pteridic acids H and F (2 mL, 1.0 ng/mL for both) were added separately into corresponding containers, with sterile Milli-Q water as control, and an extra 8 mL of Milli-Q water was added to each petri dish every other day.

Bioinformatics analyses. The identification and annotation of all BGCs of *Streptomyces* secondary metabolites were carried out with antiSMASH 6.0.[53.] The threshold for similar BGCs was selected as greater than 45% sequence similarity. The BiG-FAM database and BiG-SCAPE software were used to identify the distribution of *pta* gene clusters in different bacteria and generate the pta-gene cluster family similarity network.[40,41] A cut-off of 0.3 was used as a raw index similarity metric for the BiG-SCAPE analysis. The alignment of 15 *pta*-containing *Streptomyces* genome sequences was performed using the whole-genome alignment plugin of the CLC Genomics Workbench version 22.0.2 (Qiagen). The minimum initial seed length was 15 bp, and the minimum alignment block length was 100 bp. The networks of Big-SCAPE and

GNPS analysis were visualised using Cytoscape 3.9. The phylogenetic analysis was conducted by the online multiple sequence alignment tool MAFFT and visualised by iTOL v5. [54,55]

Statistical analysis. Statistical significance was assessed by one-way ANOVA with *post hoc* Dunnett's multiple comparisons test. Differences at *P*-values < 0.01 were considered significant. Asterisks indicate the level of statistical significance: $^{*}P < 0.05$, $^{**}P < 0.01$, $^{***}P < 0.001$, and $^{****}P < 0.0001$.

Data availability. The gene sequences used in this study were collected by searching National Center for Biotechnology Information (NCBI) or extracting from assembled genome sequences (attached in Supplementary Materials). All genome sequences used in this study are publicly available on NCBI. All datasets generated for this study are included in the Supplementary Materials. The original data generated through this work are available upon reasonable request.

References

1. Naylor, R., et al. A 20-year retrospective review of global aquaculture. *Nature* **591**, 551-563 (2021)
2. Wheeler, T. & von Braun, J. Climate change impacts on global food security. *Science* **341**, 508-513 (2013)
3. Zhang, H., Zhu, J., Gong, Z. & Zhu, J. Abiotic stress responses in plants. *Nat. Rev. Genet.* **23**, 104-119 (2022)
4. Kuromori, T., Fujita, M., Takahashi, F., Yamaguchi-Shinozaki, K. & Shinozaki, K. Inter-tissue and inter-organ signaling in drought stress response and phenotyping of drought tolerance. *Plant J.* **109**, 342-358 (2022)
5. Dos Santos, V., et al. Causes of reduced leaf-level photosynthesis during strong El Nino drought in a Central Amazon forest. *Global Change Biol.* **24**, 4266-4279 (2018)
6. Waadt, R., et al. Plant hormone regulation of abiotic stress responses. *Nat. Rev. Mol. Cell Biol.* **23**, 680-694 (2022)
7. Kerchev, P. & Van Breusegem, F. Improving oxidative stress resilience in plants. *Plant J.* **109**, 359-372 (2022)
8. Abid, M., et al. Physiological and biochemical changes during drought and recovery periods at tillering and jointing stages in wheat (*Triticum aestivum* L.). *Sci. Rep.* **8**, 1-15 (2018)
9. Hasanuzzaman, M., et al. Regulation of ROS metabolism in plants under environmental stress: a review of recent experimental evidence. *Int. J. Mol. Sci.* **21**, (2020)
10. Van Zelm, E., Zhang, Y. & Testerink, C. Salt tolerance mechanisms of plants. *Annu. Rev. Plant Biol.* **71**, 403-433 (2020)
11. Corwin, D. Climate change impacts on soil salinity in agricultural areas. *Eur. J. Soil Sci.* **72**, 842-862 (2021)
12. Hong, Y., Zhou, Q., Hao, Y. & Huang, A. C. Crafting the plant root metabolome for improved microbe-assisted stress resilience. *New Phytol.* **234**, 1945-1950 (2022)
13. De Vries, F., Griffiths, R., Knight, C., Nicolitch, O. & Williams, A. Harnessing rhizosphere microbiomes for drought-resilient crop production. *Science* **368**, 270-274 (2020)
14. Arif, I., Batool, M. & Schenk, P. Plant Microbiome Engineering: Expected Benefits for Improved Crop Growth and Resilience. *Trends Biotechnol.* **38**, 1385-1396 (2020)
15. Berlanga-Clavero, M., et al. Bacillus subtilis biofilm matrix components target seed oil bodies to promote growth and anti-fungal resistance in melon. *Nat. Microbiol.* **7**, 1-15 (2022)
16. Das, P., et al. Plant-soil-microbes: A tripartite interaction for nutrient acquisition and better plant growth for sustainable agricultural practices. *Environ. Res.* **214**, (2022)
17. Hiruma, K., et al. Root endophyte colletotrichum tofieldiae confers plant fitness benefits that are phosphate status dependent. *Cell* **165**, 464-474 (2016)
18. Henneron, L., Kardol, P., Wardle, D., Cros, C. & Fontaine, S. Rhizosphere control of soil nitrogen cycling: a key component of plant economic strategies. *New Phytol.* **228**, 1269-1282 (2020)
19. Etalo, D., Jeon, J. & Raaijmakers, J. Modulation of plant chemistry by beneficial root microbiota. *Nat. Prod. Rep.* **35**, 398-409 (2018)
20. Quinn, G., Banat, A., Abdelhameed, A. & Banat, I. Streptomyces from traditional medicine: sources of new innovations in antibiotic discovery. *J. Med. Microbiol.* **69**, 1040-1048 (2020)
21. Viaene, T., Langendries, S., Beirinckx, S., Maes, M. & Goormachtig, S. Streptomyces as a plant's best friend? *FEMS Microbiol. Ecol.* **92**, (2016)
22. Myo, E., et al. Indole-3-acetic acid production by *Streptomyces fradiae* NKZ-259 and its formulation to enhance plant growth. *BMC Microbiol.* **19**, 1-14 (2019)
23. Sadeghi, A., et al. Plant growth promoting activity of an auxin and siderophore producing isolate of Streptomyces under saline soil conditions. *World J. Microbiol. Biotechnol.* **28**, 1503-1509 (2012)
24. Singh, S. & Gaur, R. Endophytic *Streptomyces* spp. underscore induction of defense regulatory genes and confers resistance against *Sclerotium rolfsii* in chickpea. *Biol. Control* **104**, 44-56 (2017)
25. Fitzpatrick, C., et al. Assembly and ecological function of the root microbiome across angiosperm plant species. *Proc. Natl. Acad. Sci. U. S. A.* **115**, E1157-E1165 (2018)
26. Hamedi, J., et al. *Streptomyces iranensis* sp. nov., isolated from soil. *Int. J. Syst. Evol. Microbiol.* **60**, 1504-1509 (2010)
27. Lu, Z. & Neumann, P. Water-stressed maize, barley and rice seedlings show species diversity in mechanisms of leaf growth inhibition. *J. Exp. Bot.* **49**, 1945-1952

(1998)
28. Igarashi, Y., Iida, T., Yoshida, R. & Furumai, T. Pteridic acids A and B, novel plant growth promoters with auxin-like activity from *Streptomyces hygroscopicus* TP-A0451. *J. Antibiot.* **55**, 764-767 (2002)
29. Nong, X., Wei, X. & Qi, S. Pteridic acids C-G spirocyclic polyketides from the marine-derived *Streptomyces* sp. SCSGAA 0027. *J. Antibiot.* **70**, 1047-1052 (2017)
30. Zhu, J. Abiotic Stress Signaling and Responses in Plants. *Cell* **167**, 313-324 (2016)
31. Lavenus, J., et al. Lateral root development in Arabidopsis: fifty shades of auxin. *Trends Plant Sci.* **18**, 455-463 (2013)
32. Kautsar, S., et al. MIBiG 2.0: a repository for biosynthetic gene clusters of known function. *Nucleic Acids Res.* **48**, D454-D458 (2020)
33. Sun, P., et al. Spiroketal formation and modification in avermectin biosynthesis involves a dual activity of AveC. *J. Am. Chem. Soc.* **135**, 1540-1548 (2013)
34. Tong, Y., et al. Highly efficient DSB-free base editing for streptomycetes with CRISPR-BEST. *Proc. Natl. Acad. Sci. U. S. A.* **116**, 20366-20375 (2019)
35. Netzker, T., et al. An efficient method to generate gene deletion mutants of the rapamycin-producing bacterium *Streptomyces iranensis* HM 35. *Appl. Environ. Microbiol.* **82**, 3481-3492 (2016)
36. Gerlitz, M., Hammann, P., Thiericke, R. & Rohr, J. The biogenetic origin of the carbon skeleton and the oxygen atoms of elaiophylin, a symmetric macrodiolide antibiotic. *J. Org. Chem.* **57**, 4030-4033 (1992)
37. Haydock, S., Mironenko, T., Ghoorahoo, H. & Leadlay, P. The putative elaiophylin biosynthetic gene cluster in *Streptomyces* sp. DSM4137 is adjacent to genes encoding adenosylcobalamin-dependent methylmalonyl CoA mutase and to genes for synthesis of cobalamin. *J. Biotechnol.* **113**, 55-68 (2004)
38. Zhou, Y., Prediger, P., Dias, L., Murphy, A. & Leadlay, P. Macrodiolide Formation by the Thioesterase of a Modular Polyketide Synthase. *Angew. Chem. Int. Ed.* **54**, 5232-5235 (2015)
39. Du, L. & Lou, L. PKS and NRPS release mechanisms. *Nat. Prod. Rep.* **27**, 255-278 (2009)
40. Kautsar, S., Blin, K., Shaw, S., Weber, T. & Medema, M. BiG-FAM: the biosynthetic gene cluster families database. *Nucleic Acids Res.* **49**, D490-D497 (2021)
41. Navarro-Munoz, J., et al. A computational framework to explore large-scale biosynthetic diversity. *Nat. Chem. Biol.* **16**, 60-68 (2020)
42. Vergnes, S., et al. Phyllosphere colonization by a soil *Streptomyces* sp. promotes plant defense responses against fungal infection. *Mol. Plant-Microbe Interact.* **33**, 223-234 (2020)
43. Li, X., Tian, Y., Peng, H., He, B. & Gao, K. Isolation, screening and identification of anantagonistic actinomycetes to control Fusarium wilt of *Momordica charantia*. *Ying Yong Sheng Tai Xue Bao* **31**, 3869-3879 (2020)
44. Yun, T., et al. Anti-Foc RT4 activity of a newly isolated *Streptomyces* sp. 5-10 from a medicinal plant (*Curculigo capitulata*). *Front. Microbiol.* **11**, 610698 (2021)
45. Wang, M., et al. Sharing and community curation of mass spectrometry data with Global Natural Products Social Molecular Networking. *Nat. Biotechnol.* **34**, 828-837 (2016)
46. McDonald, B. & Currie, C. Lateral gene transfer dynamics in the ancient bacterial genus *Streptomyces*. *Mbio* **8**, e00644-17 (2017)
47. Chase, A., Sweeney, D., Muskat, M., Guillen-Matus, D. & Jensen, P. Vertical inheritance facilitates interspecies diversification in biosynthetic gene clusters and specialized metabolites. *Mbio* **12**, e02700-21 (2021)
48. Chung, Y., et al. Comparative genomics reveals a remarkable biosynthetic potential of the *Streptomyces* phylogenetic lineage associated with rugose-ornamented spores. *Msystems* **6**, e00489-21 (2021)
49. Jiang, M., et al. GdmRIII, a TetR Family Transcriptional Regulator, Controls Geldanamycin and Elaiophylin Biosynthesis in *Streptomyces autolyticus* CGMCC0516. *Sci. Rep.* **7**, (2017)
50. He, W., et al. Crossregulation of rapamycin and elaiophylin biosynthesis by RapH in *Streptomyces rapamycinicus*. *Appl. Microbiol. Biotechnol.* **106**, 2147-2159 (2022)
51. Raaijmakers, J. & Kiers, E. Rewilding plant microbiomes. *Scinece* **378**, 599-600 (2022)
52. Tsugawa, H., et al. MS-DIAL: data-independent MS/MS deconvolution for comprehensive metabolome analysis. *Nat. Methods* **12**, 523-526 (2015)
53. Blin, K., et al. antiSMASH 6.0: improving cluster detection and comparison capabilities. *Nucleic Acids Res.* **49**, W29-W35 (2021)
54. Madeira, F., et al. Search and sequence analysis tools services from EMBL-EBI in 2022. *Nucleic Acids Res.* **50**, W276-W279 (2022)
55. Letunic, I. & Bork, P. Interactive Tree Of Life (iTOL) v5: an online tool for phylogenetic tree display and annotation. *Nucleic Acids Res.* **49**, W293-W296 (2021)

Acknowledgements. We thank Yaojun Tong for the discussions on CRISPR-BEST. We thank the support from Charlotte Held Gotfredsen, DTU NMR Center, and Aaron John Christian Andersen, DTU Metabolomics Core. We thank funding support from Carlsberg Infrastructure Grant No. CF20-0177; Novo Nordisk Foundation Proof of Concept [NNF20OC0062267]; DTU Enable Program; InnoExplorer Grant, Innovation Fund Denmark; Danish National Research Foundation [DNRF137] for support towards the Center for Microbial Secondary Metabolites (CeMiSt). Zhijie Yang acknowledges funding from the China Scholarship Council [202004910340]. Tilmann Weber

acknowledges funding from the Novo Nordisk Foundation [NNF20CC0035580].

Author contributions. Zhijie Yang and Tilmann Weber carried out genetic experiments and bioinformatic analyses; Emil Strøbech isolated the metabolites and characterised the structures; Ling Ding did structure elucidation, crystalised the compounds, and did preliminary plant assays; Yijun Qiao, Naga Charan Konakall and Erik Andreasson carried out the Arabidopsis assay; Gundela Peschel and Miriam Agler-Rosenbaum carried out large scale fermentation and downstream processing; Pernille Harris did X-ray crystallography. All authors contributed to writing and reviewing the manuscript.

Competing interests. The authors declare no competing interests.

Materials & Correspondence. All correspondences and material requests should be addressed to Ling Ding.

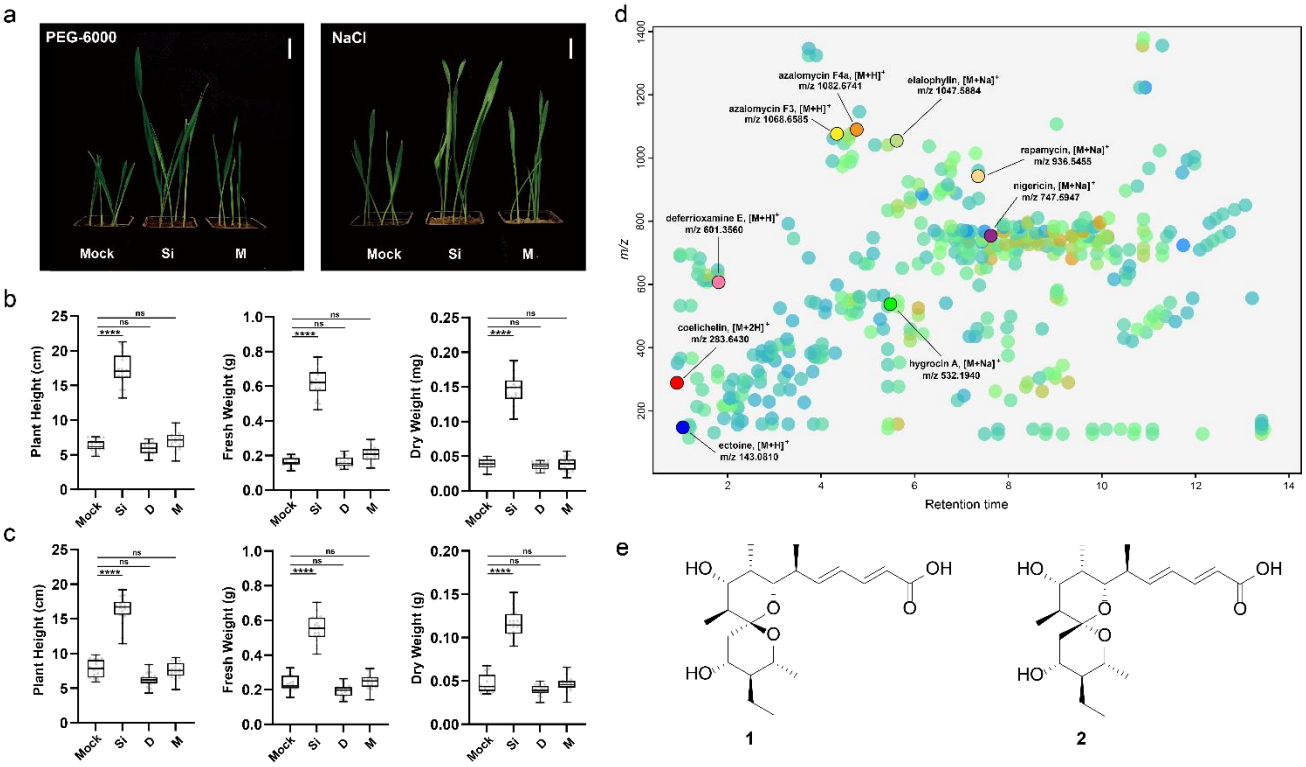

Figure 1. The effect of *S. iranensis* HM 35 on barley seedlings under the abiotic stress and the bioactive components. ***a***, *S. iranensis* HM 35 and its abiotic stress mitigated on barley (bars = 2 cm). The drought stress and salinity stress were mediated by 20% (w/v) PEG-6000 and 100 mM NaCl, respectively; ***b***, the box plot (middle bar = median, box limit = upper and lower quartile, extremes = min and max values) depicts the plant height, fresh weight and dry weight of barley seedlings growing on drought condition (n = 18); ***c***, the box-plot (middle bar = median, box limit = upper and lower quartile, extremes = min and max values) depicts the plant height, fresh weight and dry weight of barley seedlings growing on salinity condition (n = 18); ***d***, The metabolite profile of the native *S. iranensis* HM 35 growing in liquid ISP2 medium, the known secondary metabolites were identified by LC-MS/MS and highlighted; ***e***, the bioactive components pteridic acid H (**1**) and pteridic acid F (**2**) isolated from *S. iranensis* HM 35. Abbreviations: *CK*, control; *Si*, treatment of *S. iranensis* HM 35 culture broth; *D*, treatment of *S. iranensis* HM 35/Δ*ptaA* culture broth; *M*, treatment of blank medium (ISP2). Asterisks indicate the level of statistical significance: $^{*}P < 0.05$, $^{**}P < 0.01$, $^{***}P < 0.001$, and $^{****}P < 0.0001$.

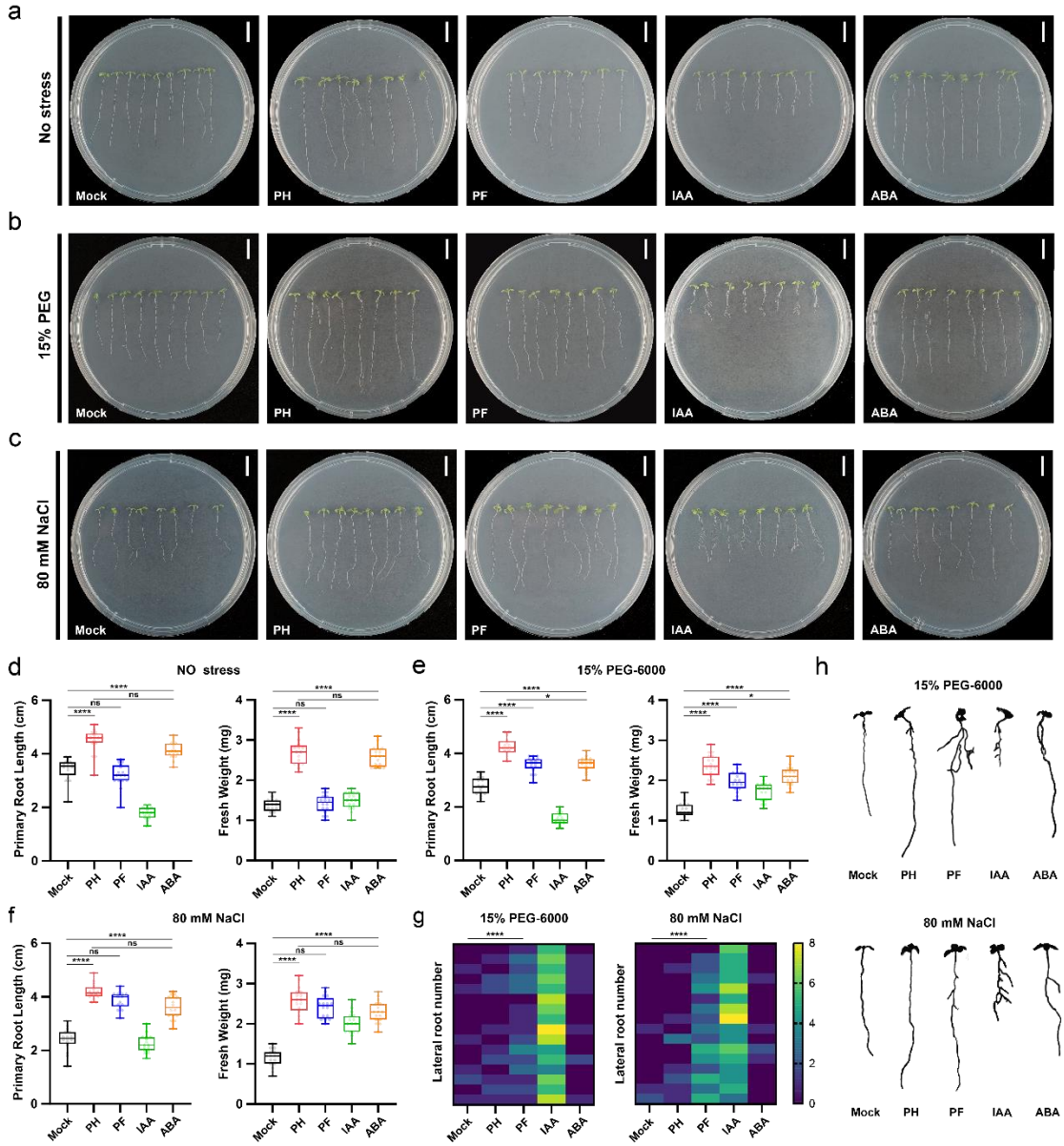

Figure 2. The effect of pteridic acids H and F on Arabidopsis seedlings under abiotic stress. ***a***, phenotype of Arabidopsis seedlings growing on modified Murashige & Skoog medium without abiotic stress using different treatments (bars = 1 cm); ***b***, phenotype of Arabidopsis seedlings growing under drought stress mediated by 15% (w/v) PEG-6000 using other treatments (bars = 1 cm); ***c***, phenotype of Arabidopsis seedlings growing under salinity stress mediated by 80 mM NaCl using other treatments (bars = 1 cm); ***d***, the box-plot (middle bar = median, box limit = upper and lower quartile, extremes = min and max values) depicts the primary root length and fresh weight of Arabidopsis seedlings growing on non-stress condition (n = 16); ***e***, the box-plot depicting the primary root length and fresh weight of *A. thaliana* seedlings growing on drought stress condition (n = 16); f, the box-plot depicting the primary root length and fresh weight of Arabidopsis seedlings growing on salinity stress condition (n = 16); ***g***, the heat map of lateral root number of Arabidopsis seedlings growing in different conditions; ***h***, the phenotype differences of lateral root growth of Arabidopsis seedlings growing in other conditions. Abbreviations: *Mock*, control; *PH*, treatment of 0.5 ng mL^{-1} pteridic acid H; *PF*, treatment of 0.5 ng mL^{-1} pteridic acid F; IAA, treatment of 1.3 nM indole-3-acetic acid; *ABA*, treatment of 1.3 nM abscisic acid. Asterisks indicate the level of statistical significance: $^{*}P < 0.05$, $^{**}P < 0.01$, $^{***}P < 0.001$, and $^{****}P < 0.0001$.

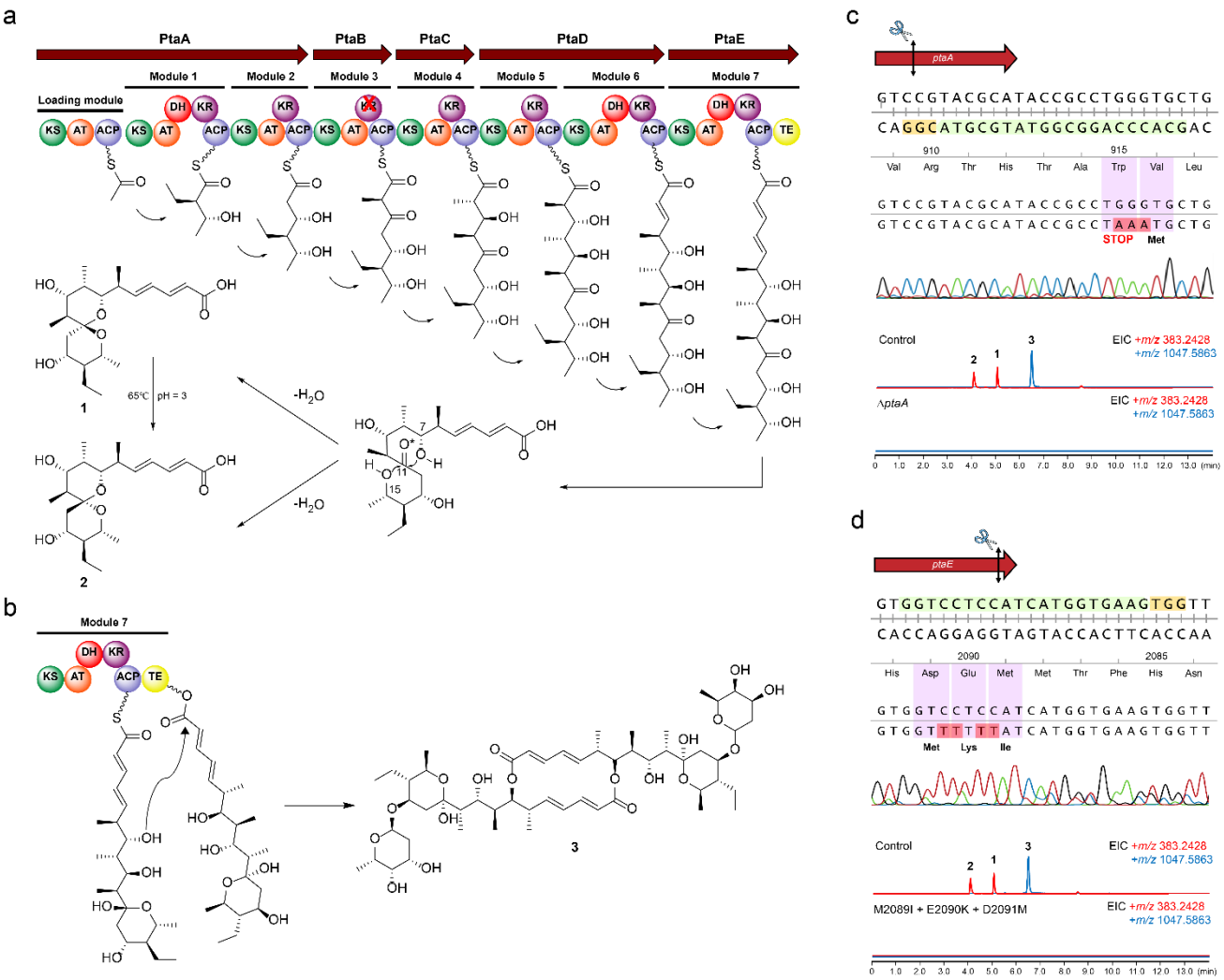

Figure 3. Biosynthesis mechanism of pteridic acids and CRISPR base editing application in *S. iranensis* HM 35. ***a***, the proposed biosynthetic pathway of pteridic acid H (**1**) and F (**2**); ***b***, the proposed biosynthesis mechanism of elaiophylin (**3**), and its macrodiolide formation is catalysed by thioesterase (TE) domain. ***c***, Sanger sequencing and LC-MS/MS output of CRISPR base editing application of STOP codon introduction targeting the *ptaA* of *S. iranensis* HM 35. The 20-nt protospacer sequence is highlighted in light green, whereas the 3-nt PAM sequence is shown in yellow. The codons and corresponding amino acids are indicated, and the black double-headed arrow represents the position of the editing window. Extracted Ion Chromatography (EIC) for **1** and **2** (*m/z* 383.2428 $[M+H]^+$) and **3** (*m/z* 1047.5863 $[M+Na]^+$) in the wild type *S. iranensis* HM 35 (Control) and the mutant *S. iranensis* HM 35/Δ*ptaA* (Δ*ptaA*); ***d***, Sanger sequencing and LC-MS/MS output of CRISPR base editing application of site-directed mutagenesis targeting the TE domain of *pta* BGC. EIC for **1** an **2** (*m/z* 383.2428 $[M+H]^+$) and **3** (*m/z* 1047.5863 $[M+Na]^+$) in the wild type *S. iranensis* HM 35 (Control) and the mutant *S. iranensis* HM 35 (M2089I + E2090K + D2091M).

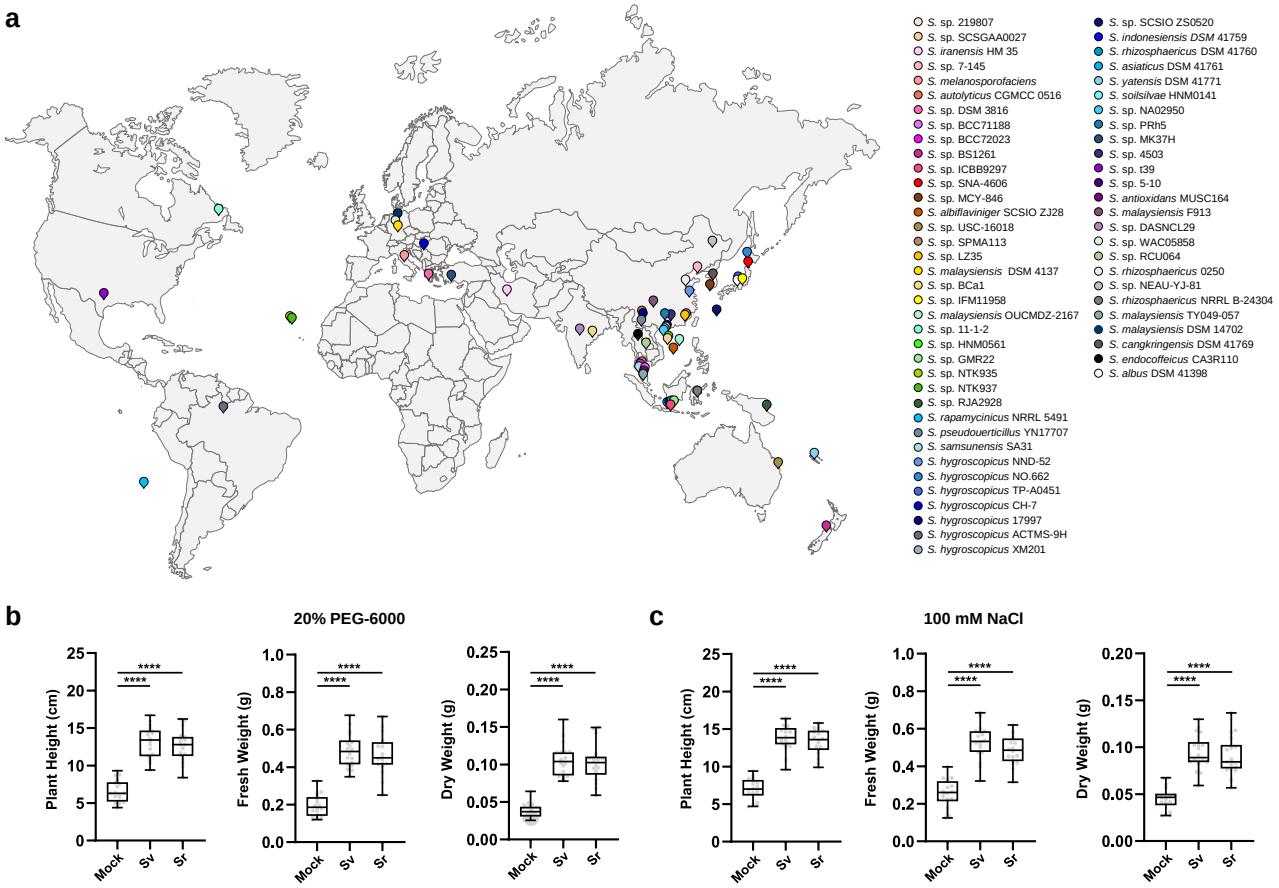

Figure 4. Geographical distribution of *pta*-containing *Streptomyces* strains and abiotic stresses alleviation activity testing of *S. violaceusniger* Tu 4113 and *S. rapamycinicu*s NRRL 5491. ***a***, the global geographic distribution of *Streptomyces* strains possessing *pta* BGC. A total of 60 *Streptomyces* strains were displayed on the map and distinguished by different colours. For detailed strain information, see Supplementary Tab. S4; ***b***, Different growth of barley seedlings in drought stress mediated by 20% (w/v) PEG-6000; ***c***, Different growth of barley seedlings in drought stress mediated by 100 mM NaCl. Abbreviation: *Mock*, control; *Sv*, treatment of *S. violaceusniger* Tu 4113; *Sr*, treatment of *S. rapamycinicus* NRRL 5491. Asterisks indicate the level of statistical significance: $^{*}P < 0.05$, $^{**}P < 0.01$, $^{***}P < 0.001$, and $^{****}P < 0.0001$.

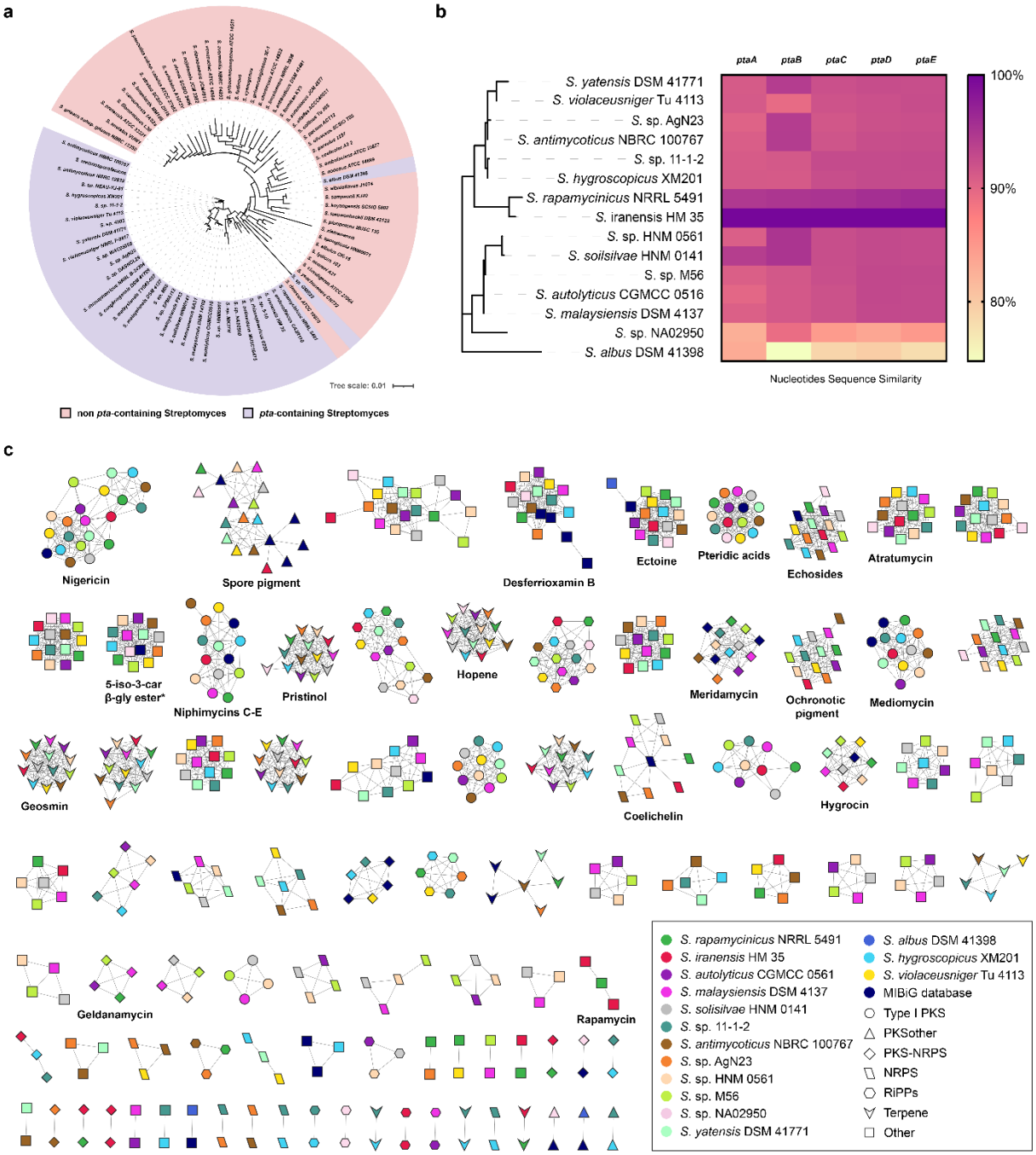

Figure 5. The phylogenetic and secondary metabolites BGCs analysis of *pta*-containing *Streptomyces* strains. ***a***, the phylogenetic tree of 16S rRNA nucleotides sequences of *pta*-containing *Streptomyces* and other *Streptomyces* strains; ***b***, the heatmap depicts similarity differences of core genes of *pta* BGC between *S. iranensis* HM 35 and other 14 *pta*-containing *Streptomyces* strains; ***c***, the secondary metabolites BGCs similarity network of 15 *pta*-containing *Streptomyces* strains with complete genome information. Different strains and types of secondary metabolites are represented by different colours and shapes, respectively. *, 5-isoprenylindole-3-carboxylate β-glycosyl ester.